atmosphere

MDPI

*Article*

# Hydrothermal Controls of Climate Extremes on Maize Yield Across Scales in Hilly Regions

**Yinxi Zhao [1], Yanzai Wang [1,*], Heng Wang [2] and Yang Wang [1]**

[1] College of Geography and Tourism, Chongqing Normal University, Chongqing 401331, China
[2] College of Urban and Environmental Sciences, Northwest University, Xi'an 710127, China
* Correspondence: wyz2003qu@163.com

**Abstract**

This study examines the multi-scale relationships between extreme climate indices and maize yield from a hydrothermal perspective, across both temporal (long-term trends, interannual anomalies, and abrupt changes) and spatial (regional and grid) scales in the Chengdu–Chongqing region, using long-term meteorological (1985–2025) and crop yield (1982–2015) datasets. Results reveal pronounced warming and drying trends, characterized by increasing warm-related temperature extremes and consecutive dry days, along with a decline in cold extremes. A shift toward drier conditions occurred around 2005, while temperature extremes have exhibited stepwise changes since the late 1990s. Maize yield shows a significant upward trend with an abrupt increase around 1997, closely linked to reduced cold stress. Scale-dependent analyses reveal that climate-yield relationships are primarily expressed through long-term hydrothermal changes rather than short-term variability, with maize yield showing positive responses to warm conditions and prolonged dry spell duration, and negative responses to cold extremes and excessive precipitation. In contrast, relationships based on interannual anomalies are weak and spatially inconsistent, suggesting limited sensitivity of yield to short-term climate variability due to system buffering and agricultural adaptation. Spatially, climate–yield relationships exhibit marked heterogeneity, with temperature constraints dominating in the western region and moisture-related effects being more pronounced in the central–eastern basin. Mechanistically, abrupt change analysis indicates two distinct controls: cold extremes act as threshold constraints associated with rapid yield shifts, whereas warming and drying exert gradual cumulative effects on productivity. Overall, maize yield dynamics are more strongly associated with long-term hydrothermal evolution than interannual variability, highlighting the importance of distinguishing temporal scales, hydrothermal regimes and long-term agricultural system evolution in climate–crop assessments under ongoing climate change.

**Keywords:** extreme climate indices; maize yield; climate change; spatial heterogeneity



Academic Editor: Gianni Bellocchi

Received: 19 April 2026
Revised: 27 May 2026
Accepted: 3 June 2026
Published: 5 June 2026



## 1. Introduction

Global warming is posing increasing challenges to agricultural production worldwide [1]. The global mean surface temperature has increased by approximately 1 °C above pre-industrial levels and continues to rise at a rate of about 0.2 ± 0.1 °C per decade [2]. In China, the warming trend is even more pronounced, reaching 0.26 °C per decade during 1951–2020, exceeding the global average [3,4]. This warming has been accompanied by an increasing frequency and intensity of extreme climate events, including heatwaves,

droughts, and floods, particularly in ecologically sensitive regions such as Southwest China [5–7].

Meanwhile, the potential for expanding cultivated land in China is limited, making yield improvement per unit area a key pathway for ensuring food security [8,9]. Maize, one of the most important staple crops globally, plays a crucial role in this context. Therefore, understanding how extreme climate variability affects maize production is of critical importance. Depending on regional conditions and crop varieties, climate variability may produce either positive or negative effects on maize yield [5].

Previous studies have employed various approaches to assess the climate impacts on crop yields, including process-based crop models, statistical analyses, and field experiments [5,10–13]. These studies indicate that climate change can exert both beneficial and adverse effects on crop production [5]. For instance, global warming has been associated with significant yield reductions, with maize yields decreasing by approximately 7.5% per °C increase in temperature [14]. However, considerable spatial heterogeneity exists, and in some regions warming may extend the growing seasons or increase cropping intensity, partially offsetting negative impacts [15].

Climate change affects crop yields through multiple pathways, including heat stress, drought stress, and compound extreme events. High temperatures during critical growth stages, particularly flowering and grain filling, can reduce pollen viability and disrupt pollination, leading to yield losses [16–18]. In addition, compound dry–hot events can amplify these effects, resulting in more severe reductions in maize production [19,20]. These interacting processes introduce substantial uncertainty in crop responses to climate variability.

Despite these advances, most existing studies have focused on the magnitude and mechanisms of climate impacts, while relatively limited attention has been given to the temporal consistency between extreme climate changes and crop yield dynamics. In particular, it remains unclear whether trends and abrupt changes in extreme climate indices are synchronized with those of maize yield, or whether temporal mismatches and time lag effects exist across different spatial scales.

The Chengdu–Chongqing area, located in the western hilly region of western China [21], is highly sensitive to climate variability due to its complex terrain and reliance on rainfed agriculture. Since the late 1990s, this region has experienced a significant increase in extreme warm events and compound dry–hot extremes, including severe droughts in 2006 and during 2009–2011, which caused substantial agricultural losses [6,22–25]. However, systematic assessments of the co-evolution of extreme climate indices and maize yield in this region remain limited.

To address this gap, this study conducts a multi-scale assessment of extreme climate indices and maize yield in the Chengdu–Chongqing region. Using long-term meteorological data (1985–2025) and maize yield data (1982–2015), we (1) quantify temporal trends using the Mann–Kendall test and the Theil–Sen slope estimator, (2) detect abrupt changes using the Pettitt test, and (3) evaluate the consistency between climate extremes and maize yield at both regional and grid scales. This study aims to provide new insights into climate-crop interactions, thereby supporting agricultural adaptation under climate change.

## 2. Study Area

The Chengdu–Chongqing area is located in the upper reaches of the Yangtze River within the Sichuan Basin of southwestern China, covering an area of ~185,000 km$^2$ and including the central urban districts and 27 counties of Chongqing Municipality as well as 15 cities in Sichuan Province [26].

Topographically, the region lies on the second step of China's three-tiered terrain and exhibits complex and diverse landforms. It is surrounded by mountains and plateaus,

while the central basin consists mainly of plains and low hills with an average elevation of 200–500 m a.s.l. [27]. The study area extends from the Wumeng Mountains in the south to the Qinling Mountains in the north, and from the Min-Daliang Mountain in the west to the Daba–Wushan Mountains in the east, forming a distinct pattern of elevated margins and a low-lying central basin (Figure 1).

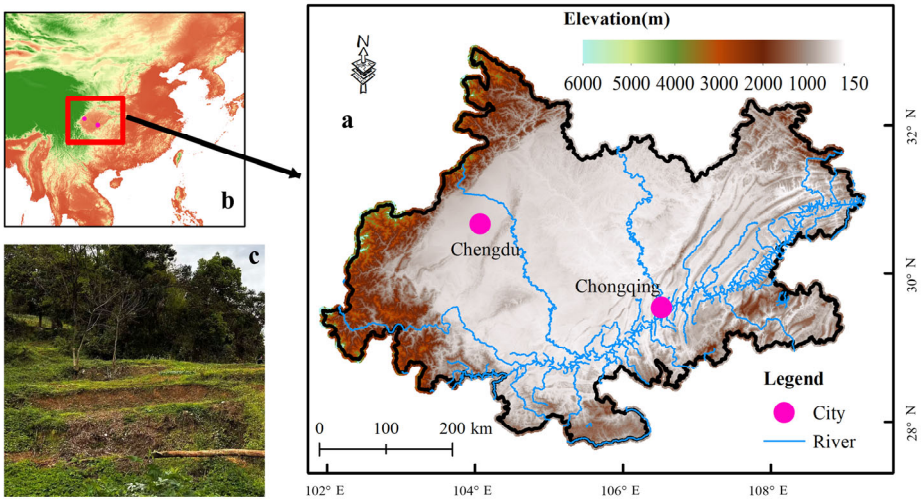


**Figure 1.** Study area and hilly croplands. (**a**) Topographic characteristics of the Sichuan Basin. (**b**) Geographic location of the Chengdu–Chongqing region within China. (**c**) Field photograph of representative hillslope croplands in the study area.

The Sichuan Basin is characterized by a humid and cloud-prone climate, with high relative humidity, frequent cloud cover, and limited sunshine duration [28]. These conditions are strongly influenced by the surrounding basin topography, which promotes water vapor convergence and frequent fog formation [29]. As a result, the region exhibits relatively low surface solar radiation compared to other regions at similar latitudes.

Agricultural resources show strong spatial heterogeneity due to geomorphological differences. The Sichuan portion is dominated by fertile alluvial plains with abundant arable land, while the Chongqing portion is characterized by more complex terrain, including hills, mountains, and karst landscapes [21,30]. By 2022, the cultivated land area reached ~10.6 million hectares, with a land reclamation rate of 28.6%, making the region an important national grain production base [27]. Agriculture in hilly and mountainous areas is largely based on rainfed systems [31]. Maize cultivation on sloping farmland primarily depends on natural precipitation, with relatively limited management inputs such as fertilization and weed control, making crop production highly sensitive to climate variability and extreme events. Based on a 30 m resolution maize distribution dataset for 2015 [32], maize cultivation covered approximately 6.99% of the total study area. Despite the highly fragmented nature of hillslope croplands in the Chengdu–Chongqing region, maize cultivation remains widely distributed across the study area.

## 3. Data Sources and Methods

### *3.1. Data Sources and Preprocess*

The meteorological data used in this study were obtained from the agrometeorological indicators reanalysis dataset (1985–2025) provided by the Copernicus Climate Change Service (accessed on 5 March 2025) [33]. The dataset has a horizontal resolution of 0.1° × 0.1° and a daily temporal resolution. We extracted daily precipitation flux (mm/day), daily maximum temperature (K), and daily minimum temperature (K). Extreme temperature

and precipitation indices were calculated following the definitions of the Expert Team on Climate Change Detection and Indices (ETCCDI) [34] (Table 1).

**Table 1.** Definition of Extreme climate indices [34].

| Category | Index | Name | Definition | Unit |
|---|---|---|---|---|
| Extreme temperature index | FD | Frost days | Annual count of days when TN < 0 °C | days |
| | SU | Summer days | Annual count of days when TX > 25 °C | days |
| | TN10p | Cool nights | Percentage of days when TN < 10th percentile | % |
| | TX10p | Cool days | Percentage of days when TX < 10th percentile | % |
| | TN90p | Warm nights | Percentage of days when TN > 90th percentile | % |
| | TX90p | Warm days | Percentage of days when TX > 90th percentile | % |
| | TNn | Min Tmin | Annual minimum value of TN | °C |
| | TXx | Max Tmax | Annual maximum value of TX | °C |
| Extreme precipitation index | CDD | Consecutive dry days | Maximum number of consecutive days with RR < 1 mm | days |
| | CWD | Consecutive wet days | Maximum number of consecutive days with RR ≥ 1 mm | days |
| | R10 | Heavy precipitation days | Annual count of days when RR ≥ 10 mm | days |
| | R20 | Very heavy precipitation days | Annual count of days when RR ≥ 20 mm | days |
| | R95p | Very wet days | Annual total precipitation when RR > 95th percentile | mm |
| | R99p | Extremely wet days | Annual total precipitation when RR > 99th percentile | mm |
| | RX1day | Max 1-day precipitation amount | Annual maximum 1-day precipitation | mm |
| | SDII | Simple daily intensity index | Annual total precipitation divided by the number of wet days (RR ≥ 1 mm) | mm/day |
| | PRCPTOT | Annual total precipitation | Annual total precipitation in wet days (RR ≥ 1 mm) | mm |

RR: daily precipitation amount (mm/day); TX: daily maximum temperature (°C); TN: daily minimum temperature.

Maize yield data were obtained from the Global Major Cereal Crop Yield Dataset (1982–2015) [35], provided by the National Ecosystem Science Data Center. The dataset has a horizontal resolution of 5 arc-min (approximately 10 km × 10 km) and an annual temporal resolution, with maize yield expressed in kg/ha.

For trend and abrupt change analyses, extreme climate indices and maize yield were analyzed using their native spatial resolutions. For correlation analysis, the two datasets were treated differently depending on the scale of analysis. At the regional scale, correlations between extreme climate indices and maize yield were calculated using their respective time series without spatial resampling. At the grid scale, however, the extreme climate indices were first resampled to a 10 km × 10 km resolution to match the maize

yield dataset, and Spearman rank correlation was then performed between each extreme climate index and maize yield for each grid cell.

Due to differences in temporal coverage between the climate dataset (1985–2025) and the maize yield dataset (1982–2015), different time windows were adopted for different types of analyses. Specifically, trend detection and abrupt change analyses were conducted using the full available time series for each dataset to maximize the robustness of long-term signal detection. In contrast, for correlation analysis and trend consistency assessment between extreme climate indices and maize yield, only the overlapping period (1985–2015) was used to ensure temporal comparability and avoid spurious relationships arising from mismatched time spans.

### *3.2. Trend Detection*

In this study, we conducted trend analyses of extreme climate indices and maize yield in the Chengdu–Chongqing region at both the regional (whole-area) and grid scales using Theil–Sen slope [36], Mann–Kendall trend test [37], and Pettitt abrupt change test [38]. At the regional scale, annual spatial averages of all grids within the study area were calculated for each climate index and maize yield, generating time series spanning multiple decades. The Theil–Sen slope and Mann–Kendall test were then applied to these time series to quantify the overall trends, while the Pettitt test was used to detect abrupt change years. At the grid scale, time series were extracted for each grid cell, and the same methods were applied to evaluate local trends and abrupt changes. This approach allowed us to derive both the spatial distribution of Theil–Sen slopes and the spatial pattern of abrupt change years for extreme climate indices and maize yield across the study area.

(1) Theil-Sen slope estimation

The Theil–Sen slope estimator is a non-parametric method used to quantify the magnitude of a trend in a time series [36]. It calculates the slopes between all pairs of observations in the time series and uses the median of these pairwise slopes as a robust estimate of the overall trend. The formula for the Theil–Sen slope is given as follows:

$$S\_slope = median\left(\frac{x_j - x_i}{j - i}\right),\ i < j \tag{1}$$

where $S\_slope$ represents the Theil–Sen estimator, defined as the median of the slopes calculated from all pairs of observations in the sample. The magnitude of $S\_slope$ indicates the strength of the trend: A positive value denotes an increasing trend, whereas a negative value indicates a decreasing trend over the study period. $x_j$ and $x_i$ represent observations at times $i$ and $j$, respectively.

However, the Theil–Sen estimator alone does not evaluate the statistical significance of the detected trend. Therefore, it is commonly used in combination with the Mann–Kendall Trend Test, which is applied to assess the significance of monotonic trends in a time series.

(2) Mann–Kendall trend test

The Mann–Kendall Trend test is a non-parametric statistical method widely used to detect monotonic trends in hydroclimatic time series [37]. For a given time series $x_j = (x_1, x_2, \ldots, x_n)$, the test statistic S is defined as:

$$S = \sum_{j=1}^{n-1} \sum_{k=j+1}^{n} sgn(x_k - x_j) \tag{2}$$

where $n$ denotes the sample size and sgn is the sign function defined as:

$$sgn(x_k - x_j) = \begin{cases} 1\ x_k - x_j > 0 \\ 0\ x_k - x_j = 0 \\ -1\ x_k - x_j < 0 \end{cases} \tag{3}$$

when the sample size $n \geq 10$, the statistic S approximately follows a normal distribution. The variance of S is calculated as:

$$Vas(S) = \frac{n(n-1)(2n+5)}{18} \tag{4}$$

The standardized test statistic Z is calculated as:

$$Z = \begin{cases} \frac{S-1}{\sqrt{Var(S)}} & S > 0 \\ 0 & S = 0 \\ \frac{S+1}{\sqrt{Var(S)}} & S < 0 \end{cases} \tag{5}$$

The statistic Z follows a standard normal distribution. At a given significance level $\alpha$, the null hypothesis of no monotonic trend cannot be rejected if $|Z| \leq Z_{1-\alpha/2}$; otherwise, it is rejected, indicating a statistically significant trend. For significance levels of $\alpha = 0.05$ and $\alpha = 0.01$, the corresponding critical values are $Z_{1-\alpha/2}$ = 1.96 and 2.58, respectively.

(3) Pettitt abrupt change test

The Pettitt abrupt test is a non-parametric method widely used to detect a single abrupt change in the central tendency of a time series [38]. For a time series $x_1, x_2, \ldots, x_n$ of length $n$, the test statistic is based on the ranks of the observations. First, assign ranks $r_i$ to each observation $x_i$ in ascending order.

$$r_i = \begin{cases} 1 & x_i > x_j \\ 0 & x_i = x_j \\ -1 & x_i < x_j \end{cases} \tag{6}$$

where $j$-th in the time series $x_1, x_2, \ldots, x_n$. For each possible change point t ($1 \leq t < n$), the Pettitt statistic $U_t$ is defined as:

$$U_t = 2\sum_{i=1}^{t} r_i - t(n+1) \tag{7}$$

where $t$ denotes the candidate abrupt year. Then, the test identifies the change year $t^*$ at which the absolute value of $U_t$ is maximized $K = \max_{1 \leq t < n} |U_t|$. The corresponding time $t^*$ is considered the estimated abrupt change year.

Finally, the approximate $p$-value of K is calculated as: $p \approx 2\exp\left[\frac{-6K^2}{n^3+n^2}\right]$. At a given significance level $\alpha$, the null hypothesis of no change is rejected if $p < \alpha$, indicating a statistically significant abrupt shift in the time series at $t^*$. The Pettitt test is distribution-free and suitable for non-normal data. It detects only a single change point, typically in the median of the series. It is often used in combination with trend tests (e.g., Mann–Kendall) to distinguish gradual trends from abrupt regime shifts in climate and crop data.

### *3.3. Trend Consistency Analysis*

The Spearman rank correlation coefficient ($\rho$) is a non-parametric measure used to assess the strength and direction of the monotonic relationship between two variables [39]. Analyses were conducted at both the regional and grid scales.

Direct correlation analysis between raw climate variables and maize yield may be influenced by long-term trends and non-stationarity in the time series, which can confound the interpretation of climate-crop relationships. To better distinguish the effects of long-term climate change and interannual variability on maize yield, a trend-anomaly decomposition approach was adopted prior to correlation analysis.

In this study, the time series of extreme climate indices and maize yield were decomposed into trend and anomaly components using locally weighted polynomial regression

(LOESS). LOESS is a non-parametric smoothing technique that fits a smooth curve to a time series through localized regressions without assuming a predefined functional form [40]. This property makes it particularly suitable for capturing nonlinear and nonstationary trends in climate and agricultural data [41].

For a given time series $x(t)$, the decomposition can be expressed as:

$$x(t) = x_{trend}(t) + x_{anomaly}(t) \quad (8)$$

where $x_{trend}(t)$ represents the long-term trend component derived from LOESS smoothing, and $x_{anomaly}(t)$ represents the residual component defined as the deviation from the fitted trend.

Based on this decomposition, two types of correlation analyses were conducted at both the regional and grid scales over the overlapping period (1985–2015): (i) Trend correlation analysis: Spearman correlation between the trend components of climate indices and maize yield, used to evaluate the influence of long-term climate change on yield evolution. (ii) Anomaly correlation analysis: Spearman correlation between the anomaly components of climate indices and maize yield, used to assess the sensitivity of maize yield to interannual climate variability.

Statistical significance was assessed to identify meaningful associations, with $p$-values indicating the likelihood that the observed correlations could occur by chance. All correlation analyses were performed using the overlapping period (1985–2015) to ensure time span consistency between datasets.

In addition, to assess the spatial consistency of abrupt changes between maize yield and extreme climate indices at the grid scale, we calculated the difference in change-point years for each grid cell, defined as: $\Delta T = Yield_{year} - Climate_{year}$. In practice, perfect alignment of change-point years is not required due to interannual variability. Therefore, a tolerance window of $\pm 2$ years was applied, and grid cells with $|\Delta T| \leq 2$ were considered to exhibit consistent abrupt changes between climate and maize yield. This approach provides an intuitive spatial representation of the coupling between climate extremes and crop response, allowing identification of regions where maize productivity is most sensitive to abrupt climate events.

## 4. Results

### *4.1. Spatial and Temporal Variations in Extreme Precipitation Indices*

The spatial distribution of extreme precipitation indices revealed distinct patterns across the study region (Figure 2). CDD exhibited a central-high pattern, with the highest values concentrated in the northwestern part of the study area and lower values toward the margins. In contrast, the other indices generally displayed higher values along the basin margins and lower values in the central region, although the precise locations of the maximum values varied among indices. This margin-high, center-low pattern suggests that, while the magnitude and exact location of extreme events differ among indices, the overall spatial trend is broadly consistent across the study region.

These spatial patterns largely reflect the physical meaning of the indices. CDD quantifies the duration of consecutive dry days, which explains its central-high distribution [34]. By contrast, the other indices primarily characterize precipitation amount, intensity, or wet-day frequency, leading to a margin-high, center-low pattern. Thus, while the spatial contrast is consistent, the locations of extreme values differ among indices.

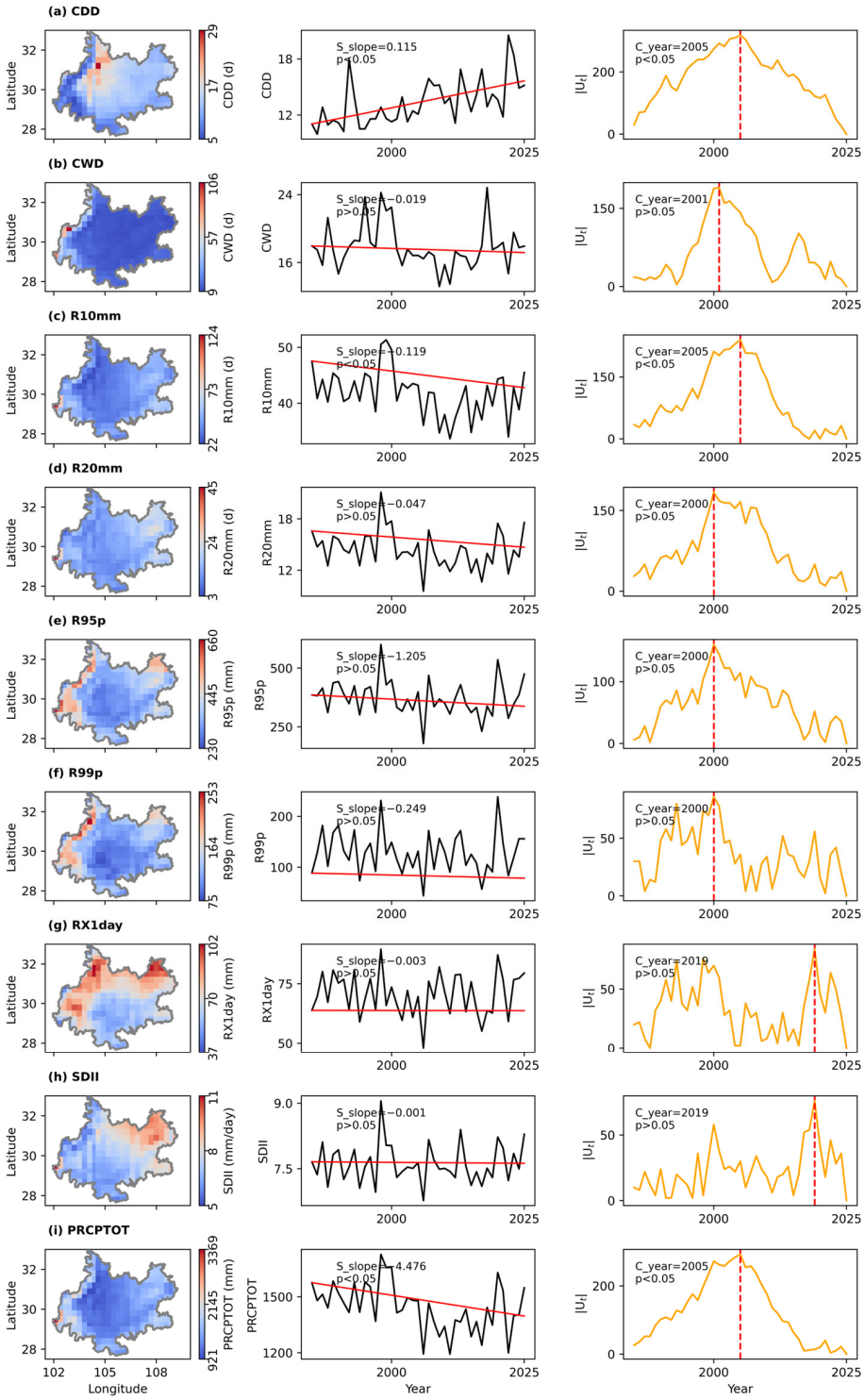


**Figure 2.** Spatial distribution, temporal trends, and abrupt changes of extreme precipitation indices in the Chengdu–Chongqing region. The left column shows the spatial distribution of the median values of each extreme precipitation index. The middle column presents temporal variations and linear trend lines estimated using Sen's slope, where the red solid lines represent the Sen's slope trends. The right column shows the abrupt change detection results based on the Pettitt test, where the red dashed vertical lines indicate the detected change-point years. $|U_t|$ represents the absolute value of the Pettitt statistics. Statistical significance was assessed at $p < 0.05$.

In terms of temporal variation over the study period (1985–2025), several indices did not exhibit significant long-term trends. Specifically, CWD, R20mm, R95p, R99p, RX1day, and SDII showed no statistically significant trends ($p > 0.05$). In contrast, CDD, R10mm,

and PRCPTOT exhibited significant trends ($p < 0.05$). Among these, CDD had a positive Sen's slope, indicating an increasing trend in consecutive dry days, whereas R10mm and PRCPTOT had negative Sen's slopes, reflecting a decline in heavy precipitation events and total precipitation. Together, these trends indicate an overall increase in dry days and a reduction in precipitation amounts over the study region.

Change-point analysis further indicated that CWD, R20mm, R95p, R99p, RX1day, and SDII did not undergo significant abrupt shifts during the study period ($p > 0.05$). For the remaining three indices, significant changes were detected around 2005: CDD, R10mm, and PRCPTOT. Prior to approximately 2005, CDD values were generally lower, increasing thereafter, while R10mm and PRCPTOT tended to decrease following this transition. These results indicate a transition from relatively wetter to drier conditions around 2005.

At the grid scale (Supplementary Figure S1), the spatial patterns of precipitation trends were further examined. Most grid cells for CWD, R20mm, R95p, R99p, RX1day, and SDII did not show significant trends ($p > 0.05$). In contrast, R10mm and PRCPTOT exhibited significant decreasing trends mainly in the northeastern part of the Sichuan Basin. Meanwhile, CDD showed significant positive trends across most of the eastern part of the study region ($p < 0.05$), indicating a pronounced increase in drought duration in the central-eastern basin.

The spatial distribution of abrupt change years (Supplementary Figure S2) showed that CWD, R20mm, R95p, R99p, RX1day, and SDII lacked significant shifts. For CDD, significant changes occurred between 1995 and 2013, with the timing shifting from earlier years in the west on to later in the east, indicating a west-to-east progression of drying. Similar patterns were observed for R10mm, while PRCPTOT showed changes mainly in the east without a clear spatial gradient.

### *4.2. Spatial and Temporal Variation in Extreme Temperature Indices*

The spatial distribution of extreme temperature indices exhibited clear regional patterns (Figure 3). FD showed higher values along the mountainous margins and lower values in the central basin, reflecting more frequent frost at higher elevations. In contrast, SU, TNn, and TXx displayed the opposite pattern, with higher values in the basin center. Percentile-based indices show more complex spatial patterns: TN90p and TX90p were higher values in the northeastern region, while TN10p and TX10p were higher in the northwest.

These patterns are primarily controlled by topography and elevation-dependent thermal processes, including temperature lapse rates, cold-air pooling within the basin, and enhanced nocturnal radiative cooling over mountainous terrain. FD reflects frost occurrence, which is enhanced at higher elevations and under stronger nocturnal cooling in the surrounding mountains, while the low-elevation central basin experiences fewer frost days. SU, TXx, and TNn indicate extreme high temperatures, which are more frequent in the basin center due to heat accumulation.

Percentile-based indices, such as TN10p, TX10p, TN90p, and TX90p, quantify the relative frequency of extreme temperature events based on local climatological thresholds. TN90p and TX90p, representing extreme hot events, reach their highest values in the northeastern part of the study area (the Three Gorges Reservoir region) and decrease toward the central and western basin, reflecting greater heat accumulation in the open northeastern basin. In contrast, TN10p and TX10p, representing extreme cold events, exhibit higher values in the central and western regions (e.g., the Chengdu Plain and the central hilly areas of the Sichuan Basin) and lower values in the northeast, consistent with stronger nocturnal cooling and lower elevations in the western basin. This interplay

between topography and local thermal dynamics underlies the observed heterogeneous spatial distribution of percentile-based temperature extremes [42].

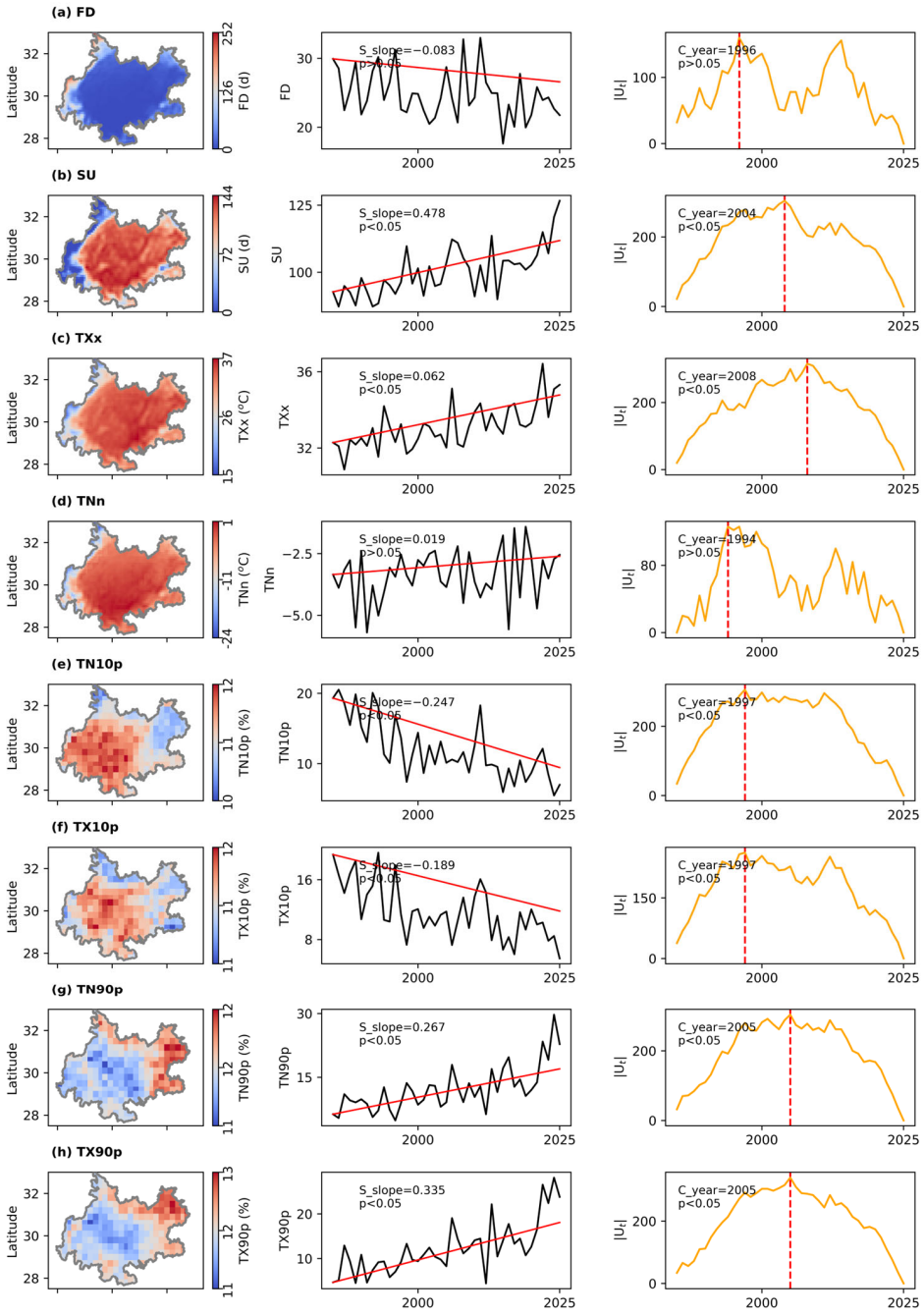


**Figure 3.** Spatial distribution, temporal trends, and abrupt changes of extreme temperature indices. The left column shows the spatial distribution of the median values of each extreme temperature index. The middle column presents temporal variations and linear trends estimate derived using Sen's slope. The right column shows the abrupt change detection results based pm the Pettitt test. In the abrupt change analysis, $|U_t|$ represents the absolute value of the Pettitt statistics. Red solid lines in the trend analysis indicate Sen's slope fitted trends, while red dashed vertical lines indicate the detected change-point years. Statistical significance was assessed at $p < 0.05$.

In terms of temporal variation during 1985–2025, frost days (FD) and the minimum of daily minimum temperature (TNn) exhibited no significant long-term trends ($p > 0.05$). In contrast, the frequency of cold events, represented by TN10p and TX10p, showed significant decreasing trends (negative Sen's slopes, $p < 0.05$), while indices associated with warm

conditions—including summer days (SU), TXx, TN90p, and TX90p—displayed significant increasing trends (positive Sen's slopes, $p < 0.05$). These results collectively indicate a pronounced warming trend, characterized by increasing hot extremes and decreasing cold extremes.

No significant abrupt changes were detected for FD and TNn over the study period. However, several other indices exhibited clear change points: TN10p and TX10p around 1997; SU, TN90p, and TX90p around 2004–2005; and TXx around These shifts suggest a stepwise transition toward warmer conditions in the Sichuan Basin, particularly since the late 1990s [43].

At the grid scale (Supplementary Figure S3), significant trends in FD and TNn were mainly confined to the western margins of the study area, while most grid cells within the basin showed no significant changes, indicating relatively stable cold extremes across the region. In contrast, TN10p and TX10p exhibited widespread negative trends across the entire study area, with stronger decreases in the western region and weaker changes toward the east, highlighting clear spatial heterogeneity in the reduction in cold events. Conversely, SU, TXx, TN90p, and TX90p all showed positive trends, with stronger warming signals in the western region that gradually weakened toward the east.

Grid-scale change-point analysis (Supplementary Figure S4) further revealed spatial heterogeneity. Significant abrupt changes in FD and TNn were primarily detected along the margins of the study area. TX90p exhibited relatively consistent change years across the region, mainly around 2011. In contrast, SU showed earlier changing year in the eastern region and later ones in the west, while TXx exhibited an earlier transition in the north and a later shift in the south. TN90p, TN10p, and TX10p generally displayed earlier changes in the western region and progressively later changes toward the east.

### *4.3. Spatial and Temporal Variation in Maize Yield*

The spatial distribution of maize yield did not show strong spatial contrasts across the study region (Figure 4). However, clear temporal trends were observed. From 1982 to 2015, maize yield exhibited a significant increasing trend, with a Sen's slope of 82.730 kg ha$^{-1}$ yr$^{-1}$. The increasing trend is consistent with that of the maize yields in China [5]. Change-point analysis revealed a significant abrupt shift around 1997 ($p < 0.05$). Before 1997, maize yield increased more rapidly, whereas after this year the growth rate slowed.

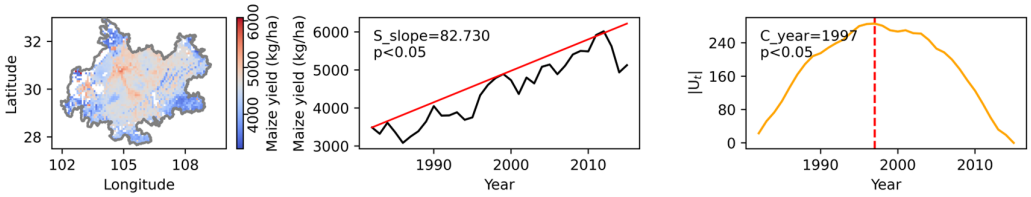


**Figure 4.** Spatial distribution, temporal trends, and abrupt changes of maize yield in the Chengdu–Chongqing region. The left column shows the spatial distribution of maize yield across the study area. The middle column presents temporal variations and linear trend estimates derived using Sen's slope. The right column shows abrupt change detection results based on the Pettitt test. In the abrupt change analysis, $|U_t|$ represents the absolute value of the Pettitt statistics. Red solid lines in the trend analysis indicate Sen's slope fitted trends, while red dashed vertical lines indicate the detected change-point years. Statistical significance was assessed at $p < 0.05$.

At the grid scale (Supplementary Figure S5), maize yield increased more slowly in the western part of the study region, particularly in the northwestern areas. In contrast, yield increases were more pronounced in the eastern part, especially in the northeastern region.

Most grid cells exhibited abrupt changes around 1995, indicating a relatively synchronous shift in maize productivity across the basin.

### *4.4. Rank Correlation Between Maize Yield and Extreme Precipitation Indices*

Maize yield exhibits markedly different relationships with extreme precipitation indices at the trend and anomaly levels. At the trend level, maize yield shows strong and statistically significant correlation with several precipitation indices (Table 2; Supplementary Figure S6). Specifically, maize yield is positively correlated with CDD ($\rho$ = 0.97, $p < 0.01$), while it is negatively correlated with CWD, R10mm, R20mm, R95p, SDII, and PRCPTOT ($p < 0.05$ or $p < 0.01$). These results indicate a robust linkage between long-term changes in precipitation regimes and maize yield evolution.

**Table 2.** Rank correlation between extreme precipitation indices and maize yield.

| | **Trends** | **Anomaly** |
|---|---|---|
| CDD | 0.97 ** | 0.13 |
| CWD | −0.58 ** | −0.04 |
| R10mm | −0.68 ** | 0.25 |
| R20mm | −0.73 ** | 0.21 |
| R95p | −0.73 ** | 0.26 |
| R99p | −0.14 | 0.21 |
| RX1day | 0.02 | 0.14 |
| SDII | −0.36 * | 0.31 |
| PRCPTOT | −0.73 ** | 0.19 |

* indicates significance at the 0.05 level; ** indicates significance at the 0.01 level.

In contrast, at the anomaly level, none of the correlation between precipitation indices and maize yield are statistically significant ($p > 0.05$; Table 2; Supplementary Figure S7). The correlation coefficients are generally weak, suggesting that interannual variability in extreme precipitation exerts only a limited influence on year-to-year fluctuations in maize yield.

Together, these findings demonstrate that the relationship between precipitation extremes and maize yield is primarily expressed through long-term co-evolutionary trends rather than short-term variability. This contrast further suggests that maize production in the study region is more strongly constrained by persistent hydroclimatic conditions than by interannual precipitation fluctuations.

At the grid scale, the relationships between extreme precipitation indices and maize yield trends exhibit pronounced spatial heterogeneity (Supplementary Figure S8). Overall, CDD shows predominantly positive correlations with yield trends across most of the study area, indicating that longer dry spells are generally associated with yield increases. In contrast, most precipitation-related indices, including CWD, R10mm, R20mm, and PRCPTOT, display mainly negative correlations, particularly over the central and eastern regions, implying that increased precipitation frequency or total amount may suppress maize yield.

Notably, R99p and RX1day exhibit a clear west–east contrast: they are positively correlated with yield trends in the western region, while negative correlations dominate in the eastern region. This pattern suggests that the effects of intense precipitation events are highly region dependent, likely reflecting spatial differences in hydroclimatic conditions or topographic settings. In addition, R95p and SDII show more complex spatial

patterns, although negative correlations still prevail overall, with only scattered areas of positive correlations.

At the anomaly level, the correlations between extreme precipitation indices and maize yield anomalies are generally weak and spatially fragmented (Supplementary Figure S9). Most grid cells exhibit non-significant relationships ($p > 0.05$), as indicated by the widespread gray areas. Statistically significant correlations are confined to limited regions, mainly in the central-northern part of the study area, and even there, the spatial extent is small, and the sign varies among indices. No coherent spatial pattern comparable to the trend-based results is observed.

In contrast to the clear and spatially structured patterns at the trend level, the anomaly-based results indicate that extreme precipitation plays a much weaker and less consistent role in explaining interannual yield variability. This discrepancy suggests that the relationships identified in the trend analysis are primarily driven by long-term co-evolution between precipitation regimes and crop yield, rather than by direct responses to short-term fluctuations. In other words, while gradual changes in precipitation conditions can systematically influence agricultural productivity, interannual variability in extreme precipitation does not constitute a stable or dominant control on yield anomalies.

### *4.5. Rank Correlation Between Maize Yield and Extreme Temperature Indices*

Maize yield exhibits markedly different relationships with extreme temperature indices at the trend and anomaly levels (Table 3; Supplementary Figure S10). At the trend level, maize yield shows strong and statistically significant correlation with most temperature indices. Specifically, maize yield is positively correlated with SU ($\rho = 0.88$, $p < 0.01$), TXx ($\rho = 0.69$, $p < 0.01$), TNn ($\rho = 0.45$, $p < 0.01$), TN90p ($\rho = 0.92$, $p < 0.01$), and TX90p ($\rho = 0.99$, $p < 0.01$), and negatively correlated with FD ($\rho = -0.49$, $p < 0.01$), TN10p ($\rho = -0.96$, $p < 0.01$), and TX10p ($\rho = -0.56$, $p < 0.01$). These results reveal a strong and coherent warming-related signal, indicating that long-term increases in warm extremes and reductions in cold extremes are closely associated with increasing maize yield.

**Table 3.** Rank correlation between extreme temperature indices and maize yield.

| | **Trends** | **Anomaly** |
|---|---|---|
| FD | −0.49 ** | 0.26 |
| SU | 0.88 ** | 0.19 |
| TXx | 0.69 ** | −0.23 |
| TNn | 0.45 * | −0.30 |
| TN10p | −0.96 ** | 0.22 |
| TX10p | −0.56 ** | 0.27 |
| TN90p | 0.92 ** | −0.11 |
| TX90p | 0.99 ** | −0.05 |

* indicates significance at the 0.05 level; ** indicates significance at the 0.01 level.

In contrast, at the anomaly level, none of the temperature indices show statistically significant correlations with maize yield ($p > 0.05$; Table 3; Supplementary Figure S11), although weak positive or negative associations are present. This suggests that interannual fluctuations in temperature extremes exert only a limited influence on year-to-year yield fluctuations.

Overall, these findings indicate that temperature plays a dominant role in shaping long-term maize yield evolution through gradual changes in thermal conditions, whereas short-term variability in temperature extremes has a comparatively minor impact.

At the grid scale, the relationships between temperature extreme indices and maize yield trends exhibit clear spatial heterogeneity across the Chengdu–Chongqing region (Supplementary Figure S12). The cold-related indices TN10p and TX10p show predominantly negative correlations, indicating that increased cold frequency is generally detrimental to yield. In contrast, warm-related indices, including SU, TXx, TN90p, and TX90p, display mainly positive correlations across most of the study areas, suggesting beneficial effects of enhanced thermal conditions.

The index TNn shows a more complex spatial pattern, with positive correlations along the margins of the study area, and largely insignificant relationships within the interior ($p > 0.05$), except for localized negative correlations in the northeastern region. Similarly, FD exhibits a pronounced west–east contrast, with negative correlations in the western region and positive correlations in the eastern region, highlighting strong spatial variability in frost-related impacts.

At the anomaly level, the relationships between temperature extremes and maize yield anomalies are generally weak and spatially fragmented (Supplementary Figure S13). Most grid cells show non-significant correlations ($p > 0.05$), indicating a lack of consistent interannual linkage. Weak negative correlations are observed for TXx, TNn, TN90p, and TX90p in a few scattered areas, whereas FD, SU, TN10p, and TX10p exhibit limited and weak positive correlations, also confined to small regions. Overall, no coherent spatial pattern emerges at the anomaly level, in sharp contrast to the structured patterns observed in the trend analysis.

### *4.6. Abrupt Change Consistency Between Maize Yield and Extreme Climate Indices*

At the global scale, we found that among all variables with significant change-point years, maize yield changes coincided with abrupt shifts in TN10p and TX10p in 1997. At the grid scale, change-point consistency analysis (Supplementary Figures S14 and S15) revealed spatial heterogeneity in these relationships. Regions where maize yield and CDD exhibited similar change years were primarily located in the central basin, whereas consistent change points with R10mm or PRCPTOT were found mainly in central and northern areas. For temperature extremes, SU showed consistency with yield changes in the central and eastern basin, while TXx, TN90p, and TX90p were mainly consistent in the western region. However, TN10p and TX10p are mainly consistent with maize field in the northern region of the study area. These patterns suggest that long-term changes in extreme temperature conditions play a key role in driving shifts in maize productivity across different parts of the basin.

## 5. Discussion

### *5.1. Extreme Climate Change in the Chengdu–Chongqing Area*

Warm-related indices such as SU and TXx show significant increasing trends ($p < 0.05$), especially in the western part of the Chengdu–Chongqing region. SU represents the frequency of warm days whereas TXx reflects the intensity of extreme high-temperature events. Therefore, the observed increases in these indices indicate not only more frequent warm conditions but also intensified heat extremes across the region. The stronger warming signals detected in the western region may be related to the higher sensitivity of elevated terrain to climate change, while heat accumulation within the basin and urban heat effects may further amplify regional thermal contrast [42,44,45]. These patterns are consistent with both global and regional warming trends, reinforcing the broader context of climate warming [46]. Extreme temperatures indices underwent significant abrupt changes around 1997 and 2002. The spatial heterogeneity in the timing of these abrupt changes reflects differing sensitivities of extreme temperature indices to climate variability, suggesting

a non-uniform and asynchronous warming process across the region. This asynchrony may lead to temporally inconsistent or lagged impacts on agricultural systems such as maize production. This temporal pattern is consistent with prior studies which found that extreme temperatures indices changed during approximately 1995–2008 [43,47,48]. Importantly, warm-related indices such as SU tend to shift earlier in the eastern region of Chengdu–Chongqing area, highlighting the non-uniform nature of regional warming and potentially leading to inconsistent or lagged impacts on maize yield [49].

Regarding precipitation extremes, CDD shows a positive trend, particularly in the central and east regions of Chengdu–Chongqing area, suggesting intensified drought duration in these regions. Extreme precipitation indices experienced significant abrupt changes around 2005, indicating a transition from relatively wetter to drier conditions across the study area. Spatially, abrupt change generally occurred earlier in the western region and later in the eastern regions, indicating a west-to-east progression of drying [50].

### *5.2. Impact of Extreme Climate Change on Maize Yield*

The combined analyses of trends, anomalies, and abrupt changes indicate that maize yield dynamics in the Sichuan Basin are primarily associated with low-frequency (long-term) hydrothermal variability rather than high-frequency (interannual) climate fluctuations. The clear contrast between strong and spatially coherent correlations at the trend level and weak, largely insignificant relationships at the anomaly level suggests a pronounced scale-dependent coupling, whereby maize yield responds mainly to cumulative climatic forcing, whereas interannual fluctuations are largely dampened by agronomic management practices and system-level adaptation.

The decomposition of the time series into trend and anomaly components further highlights the contrasting influences of long-term climatic shifts and interannual variability. This detrending procedure reduces the influence of shared long-term trajectories and allows the isolation of interannual variability. The weak and mostly insignificant correlations at the anomaly scale therefore indicate that interannual fluctuations in extreme climate indices do not exhibit a stable or consistent relationship with year-to-year variability.

It should be noted that trend-based correlations should not be interpreted as direct causality. In addition to climatic forcing, maize yield in the Chengdu–Chongqing region has undergone substantial changes driven by socio-economic and technological development. These include the widespread adoption of hybrid maize varieties, increased fertilizer inputs and continuous improvements in agronomic management. Policy-driven agricultural modernization and regional development have further enhanced production efficiency and reduced vulnerability to climatic stressors. These non-climatic factors introduce potential confounding effects in long-term trend analysis. Therefore, the observed relationships should be interpreted as the combined outcome of climate variability and a progressively evolving agricultural production system, rather than a purely climate-driven signal.

Importantly, maize in the Chengdu–Chongqing region is typically cultivated under a dual-season system, with the main growing period from late March to early July and a secondary season from late July to October. This structure leads to an integration of climate conditions across multiple growing windows, which strengthens the influence of long-term climatic trends while smoothing interannual variability.

At the long-term scale, the observed relationships point to a coupled hydrothermal regulation mechanism. Positive correlations between maize yield and warm-related indices (e.g., SU, TXx, TN90p, and TX90p), together with negative correlations with cold-related indices (TN10p and TX10p), indicate that regional warming has alleviated thermal constraints on crop growth. Increased heat accumulation, reduced cold stress, and an extended

growing season enhance crop development and biomass production, which is particularly important for maize as a thermophilic summer crop [5,51,52].

Precipitation-related results reveal a consistent signal of beneficial drying. The positive association with CDD and negative correlations with wet-related indices (e.g., CWD, R20mm, SDII, and PRCPTOT) suggest that excessive moisture, rather than water deficit, constitutes the dominant constraint in this humid basin. Frequent cloud cover and high humidity limit radiation availability and promote waterlogging, whereas moderate reductions in precipitation can improve soil aeration, alleviate root hypoxia, and enhance solar radiation, thereby supporting photosynthesis and yield formation [51]. This effect is likely mediated through changes in soil moisture conditions, which regulate the actual water availability for crop growth, particularly in mountainous and basin-upland transition zones. Together, these findings indicate that maize yield is governed by the interaction between thermal and moisture conditions, reflecting a hydrothermal balance that regulates crop growth.

The grid-scale patterns further demonstrate that these hydrothermal controls vary spatially across the basin. For precipitation extremes, the predominantly positive correlations with CDD, particularly stronger in the central and eastern regions, indicate that dry spell duration plays a more critical role in these low-lying and poorly drained areas, where alleviating excess moisture can substantially improve soil and radiation conditions [51,53–55]. In contrast, temperature-related indices show stronger positive effects in the western region. Warm-related indices (SU, TXx, TN90p, and TX90p) exhibit the highest correlations there, suggesting that thermal limitation is more pronounced, likely associated with lower baseline temperatures and stronger topographic influences. Under these conditions, warming enhances heat accumulation, accelerates phenological development, and extends the growing season, thereby exerting a stronger positive influence on maize yield [52,56,57]. Other indices show weaker or more complex spatial patterns, indicating secondary or context-dependent effects. Extreme precipitation intensity indices (e.g., R99p and RX1day) reflect a balance between beneficial moisture input and detrimental waterlogging, while cold-related indices (e.g., FD and TNn) exhibit localized influences associated with terrain-induced thermal variability such as cold-air pooling [13,58].

These spatial patterns suggest that climatic constraints on maize production may vary spatially across the Chengdu–Chongqing region, with moisture-excess-related stress appearing more important in the central-eastern basin, whereas temperature-related limitations may exert relatively stronger influences in the western region [13,51]. However, these spatial patterns should be interpreted in conjunction with ongoing socio-economic development, technological progress, and agricultural management improvements, which also substantially influence long-term maize yield dynamics.

In contrast, the weak and spatially fragmented relationships at the anomaly level indicate that interannual variability in extreme climate indices has limited influence on yield fluctuations. This reflects both the buffering capacity of the agricultural system and the cumulative nature of crop responses. Crop growth is primarily determined by seasonally integrated hydrothermal conditions rather than isolated extreme events. As a result, interannual fluctuations do not translate into consistent yield responses.

The abrupt change analysis provides further insight into the temporal mechanisms underlying these relationships. The synchronization between maize yield shifts and abrupt changes in cold-related indices (TN10p and TX10p) around 1997 suggests that cold extremes impose threshold-type constraints on crop production. Once their frequency declines below a critical level, the risk of damage during sensitive growth stages decreases sharply, leading to rapid yield increases. In contrast, warming- and drying-related indices (e.g., SU and CDD) show strong correlations with yield trends but lack synchronous change

points, indicating gradual and cumulative effects. These factors enhance productivity through progressive increases in thermal resources, improved radiation conditions, and better soil aeration [5,13,51]. It should be noted that this period also coincides with major socio-economic transitions in the region, including administrative restructuring (e.g., the establishment of Chongqing as a municipality in 1997), as well as broader processes of agricultural intensification, market-oriented reform, and technological improvement in southwestern China. These changes may have contributed to part of the observed yield increase, although they are not explicitly quantified in this study.

Overall, maize yield in the Chengdu–Chongqing area (most parts of Sichuan Basin) is shaped by scale-dependent interactions between climatic variability and agricultural system evolution. Cold extremes act as critical thresholds that can trigger abrupt shifts in productivity, whereas warming and moderate drying exert gradual controls that shape long-term yield trajectories. The dominance of trend-level relationships over anomaly-level variability highlights that long-term co-evolution between climate and agricultural systems, rather than short-term climate fluctuations alone, represents the primary driver of maize yield changes in this humid region. Because the present study primarily focuses on climatic signals derived from large-scale datasets, the relative contributions of management intensity, technological advancement, and socio-economic change could not be explicitly quantified. Future research should therefore further integrate non-climatic drivers, such as socio-economic variables, management practices, and cultivar adaptation, to better quantify the relative contributions of climate and socio-economic factors to long-term maize yield evolution. Such integration would improve the attribution of long-term yield variability and strengthen projections of crop resilience under future climate change.

## 6. Conclusions

This study provides a multi-scale assessment of extreme climate change and its impacts on maize yield in the Chengdu–Chongqing region by distinguishing long-term trends, interannual anomalies, and abrupt changes in climate extremes.

(1) Extreme climate indices show pronounced warming and drying over the study period. Warm-related temperature extremes (e.g., SU and TXx) increase significantly, while cold extremes decrease. Precipitation indices indicate a drying tendency, characterized by increasing consecutive dry days and a basin-wide transition toward drier conditions around 2005, with clear spatial heterogeneity and a combination of gradual and stepwise changes.

(2) Maize yield exhibits a significant increasing trend with an abrupt rise around 1997, closely associated with reduced cold stress, indicating that alleviation of cold extremes acts as a key threshold for yield improvement.

(3) Climate–yield relationships vary across temporal scales. Trend-based results show strong and spatially coherent associations between maize yield and hydrothermal changes, indicating the dominance of long-term climatic forcing. In contrast, anomaly-based relationships are weak and spatially inconsistent, suggesting limited sensitivity of yield to interannual climate variability due to system buffering and agricultural adaptation.

(4) Abrupt change analysis reveals two distinct mechanisms: cold extremes act as threshold constraints that trigger rapid yield shifts once their frequency declines below critical levels, whereas warming and drying exert gradual effects by enhancing thermal resources, radiation conditions, and soil moisture-related balance.

Overall, maize yield dynamics in the Chengdu–Chongqing region reflect long-term co-evolution between climate change and agricultural system development, with climate forcing exerting stronger influences at the trend level than at the interannual level. A clear spatial transition from moisture-related stress in the central–eastern basin to temperature-limited conditions in the western region highlights the need for region-specific adaptation

strategies. However, long-term yield evolution is also strongly influenced by non-climatic factors, including technological advancement, hybrid cultivar adoption, fertilizer application, mechanization, and policy-driven agricultural development. Future studies should therefore integrate climatic, technological, and socio-economic drivers to improve the attribution of yield variability and enhance projections of agricultural resilience under future climate change.

**Supplementary Materials:** The following supporting information can be downloaded at: https://www.mdpi.com/article/10.3390/atmos17060586/s1, Figure S1: Spatial patterns of trend in extreme precipitation indices; Figure S2: Spatial patterns of abrupt years for extreme precipitation indices; Figure S3: Spatial patterns of trend in extreme temperature indices; Figure S4: Spatial patterns of abrupt years for extreme temperature indices; Figure S5: Spatial patterns of changing trends and abrupt years for maize yield; Figure S6: Rank correlations between trends in extreme precipitation indices and maize yield at the regional scale; Figure S7: Rank correlations between anomalies in extreme precipitation indices and maize yield at the regional scale; Figure S8: Rank correlations between trends in extreme precipitation indices and maize yield at the grid scale; Figure S9: Rank correlations between anomalies in extreme precipitation indices and maize yield at the grid scale; Figure S10: Rank correlations between trends in extreme temperature indices and maize yield at the regional scale; Figure S11: Rank correlations between anomalies in extreme temperature indices and maize yield at the regional scale; Figure S12: Rank correlations between trends in extreme temperature indices and maize yield at the grid scale; Figure S13: Rank correlations between anomalies in extreme temperature indices and maize yield at the grid scale; Figure S14: Abrupt year consistency between extreme precipitation indices and maize yield; Figure S15: Abrupt year consistency between extreme temperature indices and maize yield.

**Author Contributions:** Conceptualization, Y.W. (Yanzai Wang); Methodology, Y.Z. and Y.W. (Yanzai Wang); Formal analysis, Y.Z., Y.W. (Yanzai Wang), H.W. and Y.W. (Yang Wang); Investigation, Y.W. (Yanzai Wang); Data curation, Y.W. (Yanzai Wang); Writing—original draft, Y.Z. and Y.W. (Yanzai Wang); Writing—review & editing, Y.Z. and Y.W. (Yanzai Wang); Visualization, Y.W. (Yanzai Wang); Supervision, Y.W. (Yanzai Wang); Funding acquisition, Y.W. (Yanzai Wang), H.W. and Y.W. (Yang Wang). All authors have read and agreed to the published version of the manuscript.

**Funding:** This work was supported by the Chongqing Natural Science Foundation (Grant Nos. CSTB2022NSCQ-MSX1535; CSTB2023NSCQ-MSX0643; and CSTB2024NSCQ-MSX0941), the Science and Technology Research Program of Chongqing Municipal Education Commission (Grant No. KJQN20220505), and the National Natural Science Foundation of China (Grant No. 42105171).

**Institutional Review Board Statement:** Not applicable.

**Informed Consent Statement:** Not applicable.

**Data Availability Statement:** The meteorological data used in this study are publicly available from https://cds.climate.copernicus.eu/datasets/sis-agrometeorological-indicators?tab=overview (accessed on 6 March 2026). Maize yield data are publicly available from https://www.nesdc.org.cn/sdo/detail?id= 67d157f57e28176b9 b452822 (accessed on 12 March 2026).

**Conflicts of Interest:** The authors declare no conflict of interest.

## References

1. Rezaei, E.E.; Webber, H.; Asseng, S.; Boote, K.; Durand, J.L.; Ewert, F.; Martre, P.; MacCarthy, D.S. Climate Change Impacts on Crop Yields. *Nat. Rev. Earth Environ.* **2023**, *4*, 831–846. [CrossRef]
2. Ren, W. A Review of Research on Extreme Heat Events in China. *Int. J. Soc. Sci. Public Adm.* **2025**, *8*, 110–115. [CrossRef]
3. Zhang, Y.; Fu, L.; Pan, J.; Xu, Y. Projected Changes in Temperature Extremes in China Using PRECIS. *Atmosphere* **2017**, *8*, 15. [CrossRef]
4. Zhang, G.-W.; Zeng, G.; Iyakaremye, V.; You, Q.-L. Regional Changes in Extreme Heat Events in China under Stabilized 1.5 °C and 2.0 °C Global Warming. *Adv. Clim. Change Res.* **2020**, *11*, 198–209. [CrossRef]

5. Piao, S.; Ciais, P.; Huang, Y.; Shen, Z.; Peng, S.; Li, J.; Zhou, L.; Liu, H.; Ma, Y.; Ding, Y.; et al. The Impacts of Climate Change on Water Resources and Agriculture in China. *Nature* **2010**, *467*, 43–51. [CrossRef]
6. Wang, C.; Chen, C.; Zhang, S.; Ma, Z.; Pang, Y. Variation Characteristics of Extreme Climate Events in Southwest China from 1961 to 2017. *Heliyon* **2023**, *9*, e19648. [CrossRef]
7. IPCC. *Intergovernmental Panel on Climate Change (Ipcc) Climate Change 2021—The Physical Science Basis: Working Group I Contribution to the Sixth Assessment Report of the Intergovernmental Panel on Climate Change*, 1st ed.; Cambridge University Press: Cambridge, UK, 2023.
8. Yang, S.; Li, D.; Liao, H.; Zhu, L.; Zhou, M.; Cai, Z. Analysis of the Balance between Supply and Demand of Arable Land in China Based on Food Security. *Sustainability* **2023**, *15*, 5706. [CrossRef]
9. Hu, Q.; Xiang, M.; Chen, D.; Zhou, J.; Wu, W.; Song, Q. Global Cropland Intensification Surpassed Expansion between 2000 and 2010: A Spatio-Temporal Analysis Based on GlobeLand30. *Sci. Total Environ.* **2020**, *746*, 141035. [CrossRef]
10. Blanc, E.; Sultan, B. Emulating Maize Yields from Global Gridded Crop Models Using Statistical Estimates. *Agric. For. Meteorol.* **2015**, *214–215*, 134–147. [CrossRef]
11. Thompson, V.; Mitchell, D.; Hegerl, G.C.; Collins, M.; Leach, N.J.; Slingo, J.M. The Most At-Risk Regions in the World for High-Impact Heatwaves. *Nat. Commun.* **2023**, *14*, 2152. [CrossRef]
12. Luo, N.; Mueller, N.; Zhang, Y.; Feng, P.; Huang, S.; Liu, D.L.; Yu, Y.; Wang, X.; Wang, P.; Meng, Q. Short-Term Extreme Heat at Flowering Amplifies the Impacts of Climate Change on Maize Production. *Environ. Res. Lett.* **2023**, *18*, 084021. [CrossRef]
13. Zhao, C.; Liu, B.; Piao, S.; Wang, X.; Lobell, D.B.; Huang, Y.; Huang, M.; Yao, Y.; Bassu, S.; Ciais, P.; et al. Temperature Increase Reduces Global Yields of Major Crops in Four Independent Estimates. *Proc. Natl. Acad. Sci. USA* **2017**, *114*, 9326–9331. [CrossRef] [PubMed]
14. Hu, T.; Zhang, X.; Khanal, S.; Wilson, R.; Leng, G.; Toman, E.M.; Wang, X.; Li, Y.; Zhao, K. Climate Change Impacts on Crop Yields: A Review of Empirical Findings, Statistical Crop Models, and Machine Learning Methods. *Environ. Model. Softw.* **2024**, *179*, 106119. [CrossRef]
15. Yang, X.; Chen, F.; Lin, X.; Liu, Z.; Zhang, H.; Zhao, J.; Li, K.; Ye, Q.; Li, Y.; Lv, S.; et al. Potential Benefits of Climate Change for Crop Productivity in China. *Agric. For. Meteorol.* **2015**, *208*, 76–84. [CrossRef]
16. Lizaso, J.I.; Ruiz-Ramos, M.; Rodríguez, L.; Gabaldon-Leal, C.; Oliveira, J.A.; Lorite, I.J.; Sánchez, D.; García, E.; Rodríguez, A. Impact of High Temperatures in Maize: Phenology and Yield Components. *Field Crops Res.* **2018**, *216*, 129–140. [CrossRef]
17. Wang, Y.; Sheng, D.; Zhang, P.; Dong, X.; Yan, Y.; Hou, X.; Wang, P.; Huang, S. High Temperature Sensitivity of Kernel Formation in Different Short Periods around Silking in Maize. *Environ. Exp. Bot.* **2021**, *183*, 104343. [CrossRef]
18. Niu, S.; Du, X.; Wei, D.; Liu, S.; Tang, Q.; Bian, D.; Zhang, Y.; Cui, Y.; Gao, Z. Heat Stress After Pollination Reduces Kernel Number in Maize by Insufficient Assimilates. *Front. Genet.* **2021**, *12*, 728166. [CrossRef]
19. Feng, S.; Hao, Z.; Zhang, X.; Hao, F. Probabilistic Evaluation of the Impact of Compound Dry-Hot Events on Global Maize Yields. *Sci. Total Environ.* **2019**, *689*, 1228–1234. [CrossRef]
20. Hao, Z.; Hao, F.; Xia, Y.; Feng, S.; Sun, C.; Zhang, X.; Fu, Y.; Hao, Y.; Zhang, Y.; Meng, Y. Compound Droughts and Hot Extremes: Characteristics, Drivers, Changes, and Impacts. *Earth-Sci. Rev.* **2022**, *235*, 104241. [CrossRef]
21. Xiang, Q.; Yu, H.; Xu, X.; Huang, H. Temporal and Spatial Differentiation of Cultivated Land and Its Response to Climatic Factors in Complex Geomorphic Areas—A Case Study of Sichuan Province of China. *Land* **2022**, *11*, 271. [CrossRef]
22. Yu, R.; Zhai, P. More Frequent and Widespread Persistent Compound Drought and Heat Event Observed in China. *Sci. Rep.* **2020**, *10*, 14576. [CrossRef]
23. Yue, Q.; Yang, Y.; Heling, W.; Runyuan, W. Analysis on Characteristics of Drought Climate Change in Southwest China in 2006. In Proceedings of the 2019 International Conference on Meteorology Observations (ICMO), Chengdu, China, 28–31 December 2019; pp. 1–7.
24. Sun, S.; Li, Q.; Li, J.; Wang, G.; Zhou, S.; Chai, R.; Hua, W.; Deng, P.; Wang, J.; Lou, W. Revisiting the Evolution of the 2009–2011 Meteorological Drought over Southwest China. *J. Hydrol.* **2019**, *568*, 385–402. [CrossRef]
25. Liu, X.; Yuan, X.; Ma, F.; Xia, J. The Increasing Risk of Energy Droughts for Hydropower in the Yangtze River Basin. *J. Hydrol.* **2023**, *621*, 129589. [CrossRef]
26. Zhou, Y.; Li, Z.; Chen, Y.; Wei, W. Evaluating the Corresponding Relationship between the Characteristics of Resource Utilization and the Level of Urbanization: A Case Study in Chengdu-Chongqing Economic Circle, China. *Environ. Sci. Pollut. Res.* **2022**, *29*, 55816–55829. [CrossRef] [PubMed]
27. Jiang, Y. Study on the Spatial Configuration and Horizontal Compensation of Cultivated Land Fallowing in Chengdu-Chongqing Twin-City Economic Circle Based on Ecological and Food Security. Master's Thesis, Chongqing Technology and Business University, Chongqing, China, 2025.
28. Lu, H.; Xie, M.; Zhuang, B.; Ma, D.; Liu, B.; Zhan, Y.; Wang, T.; Li, S.; Li, M.; Zhu, K. Impacts of Atmospheric Circulation Patterns and Cloud Inhibition on Aerosol Radiative Effect and Boundary Layer Structure during Winter Air Pollution in Sichuan Basin, China. *Atmos. Chem. Phys.* **2024**, *24*, 8963–8982. [CrossRef]

29. Gu, L.-M.; Zeng, X.-M.; Li, C.-M.; Wang, N.; Shao, S.-B.; Ullah, I. A Numerical Simulation of a Fog Event in the Sichuan Basin, China: The Sensitivity to Terrain Elevations. *Atmosphere* **2024**, *15*, 1546. [CrossRef]
30. Pan, L.; Chen, Y.; Shi, D.; Gao, J.; Jiang, Y.; Liu, F. Spatio-Temporal Evolution of Sloping Farmland and Identification of Its Erosion Risk Management and Control Zones in the Three Gorges Reservoir Area, China. *Resour. Environ. Sustain.* **2025**, *21*, 100255. [CrossRef]
31. Chen, L.; Cui, J.; Askari, M.S.; Tang, J.; Wang, Y.; Gao, M.; Zhang, X.; Zhu, B. Impacts of Extreme Climate Events on Subtropical Upland Crops: A 20-Year Case Study in the Hilly Area of Southwest China. *Agronomy* **2026**, *16*, 572. [CrossRef]
32. Peng, Q.; Shen, R.; Li, X.; Ye, T.; Dong, J.; Fu, Y.; Yuan, W. A Twenty-Year Dataset of High-Resolution Maize Distribution in China. *Sci. Data* **2023**, *10*, 658. [CrossRef]
33. Copernicus Climate Change Service. *Agrometeorological Indicators from 1979 up to 2019 Derived from Reanalysis*; OpenAIRE: Marousi, Greece, 2019.
34. Karl, T.R.; Nicholls, N.; Ghazi, A. CLIVAR/GCOS/WMO Workshop on Indices and Indicators for Climate Extremes Workshop Summary. In *Weather and Climate Extremes*; Karl, T.R., Nicholls, N., Ghazi, A., Eds.; Springer: Dordrecht, The Netherlands, 1999; pp. 3–7.
35. Cao, J.; Zhang, Z.; Luo, X.; Luo, Y.; Xu, J.; Xie, J.; Han, J.; Tao, F. Mapping Global Yields of Four Major Crops at 5-Minute Resolution from 1982 to 2015 Using Multi-Source Data and Machine Learning. *Sci. Data* **2025**, *12*, 357. [CrossRef]
36. Sen, P.K. Estimates of the Regression Coefficient Based on Kendall's Tau. *J. Am. Stat. Assoc.* **1968**, *63*, 1379–1389. [CrossRef]
37. Mann, H.B. Nonparametric Tests Against Trend. *Econometrica* **1945**, *13*, 245. [CrossRef]
38. Pettitt, A.N. A Non-Parametric Approach to the Change-Point Problem. *Appl. Stat.* **1979**, *28*, 126. [CrossRef] [PubMed]
39. Spearman, C. The Proof and Measurement of Association between Two Things. *Am. J. Psychol.* **1904**, *15*, 72. [CrossRef] [PubMed]
40. Cleveland, W.S.; Devlin, S.J. Locally Weighted Regression:An Approach to Regression Analysis by Local Fitting. *J. Am. Stat. Assoc.* **1988**, *83*, 596–610. [CrossRef]
41. Li, X.; Kato, T.; Kongsurakan, P.; Nakagawa, T.; Suzuki, A. Long-Term Crop Yield Dynamics, Stability and Sensitivities to Large-Scale Climate Oscillations across India. *Field Crops Res.* **2026**, *342*, 110462. [CrossRef]
42. Wang, Y.; Lü, Y.; Lü, D.; Yin, L.; Wang, X. Climate Change and Its Ecological Risks Are Spatially Heterogeneous in High-Altitude Region: The Case of Qinghai-Tibet Plateau. *CATENA* **2024**, *243*, 108140. [CrossRef]
43. Fang, S.; Qi, Y.; Han, G.; Li, Q.; Zhou, G. Changing Trends and Abrupt Features of Extreme Temperature in Mainland China from 1960 to 2010. *Atmosphere* **2016**, *7*, 22. [CrossRef]
44. Pepin, N.; Apple, M.; Knowles, J.; Terzago, S.; Arnone, E.; Hänchen, L.; Napoli, A.; Potter, E.; Steiner, J.; Williamson, S.N.; et al. Elevation-Dependent Climate Change in Mountain Environments. *Nat. Rev. Earth Environ.* **2025**, *6*, 772–788. [CrossRef]
45. Zhang, Y.; Xia, X.; Zhang, Y.; Jian, L. Mobilities in the Heat: Identifying Travel-Related Urban Heat Exposure and Its Built Environment Drivers Using Remote Sensing and Mobility Data in Chengdu, China. *ISPRS Int. J. Geo-Inf.* **2025**, *14*, 372. [CrossRef]
46. Rettie, F.M.; Sapkota, T.B.; Fonteyne, S.; Gardi, M.W.; Sida, T.S. Historical Trends Reveal Significant Increase in Hot-Dry Extremes in Mexico's Bajío Region. *Environ. Monit. Assess.* **2026**, *198*, 228. [CrossRef]
47. Wang, H.; Pan, Y.; Chen, Y.; Ye, Z. Linear Trend and Abrupt Changes of Climate Indices in the Arid Region of Northwestern China. *Atmos. Res.* **2017**, *196*, 108–118. [CrossRef]
48. Lu, X.; Wei, S.; Guo, Y.; Ersi, C.; Chen, D.; Zhou, Z.; Li, Y.; Dong, Y.; Tong, Z.; Liu, X.; et al. Dynamic Hazard Assessment of Compound Drought and Heat Events in Maize Based on a Soil-Temperature-Integrated Index in Songliao Plain. *Eur. J. Agron.* **2026**, *175*, 127984. [CrossRef]
49. Zhang, Y.; Fang, H.; Gu, X.; Yin, H.; Zhang, Y.; Du, Y.; Cai, H.; Li, Y. Increasing Nitrogen Application Is Predicted to Alleviate the Effects of Climate Warming on Maize Yield Reduction and Maintain the Dietary Supply of Wheat and Maize Protein. *Eur. J. Agron.* **2024**, *161*, 127396. [CrossRef]
50. Deng, Y.; Jiang, W.; He, B.; Chen, Z.; Jia, K. Change in Intensity and Frequency of Extreme Precipitation and Its Possible Teleconnection With Large-Scale Climate Index Over the China From 1960 to 2015. *JGR Atmos.* **2018**, *123*, 2068–2081. [CrossRef]
51. Ray, D.K.; Gerber, J.S.; MacDonald, G.K.; West, P.C. Climate Variation Explains a Third of Global Crop Yield Variability. *Nat. Commun.* **2015**, *6*, 5989. [CrossRef]
52. Wang, Z.; Jia, Q.; Zhang, B.; Ming, B.; Bai, L.; Wang, F.; Wang, Y.; Yu, S.; Zou, R.; Wang, Z. Unveiling the Physiological Basis of Cold Tolerance in Maize: Root Architecture, Photosynthetic Stability, and POD-Mediated Defense Under Delayed Chilling Stress. *Plants* **2026**, *15*, 517. [CrossRef]
53. Dhakar, R.; Nagar, S.; Sehgal, V.K.; Jha, P.K.; Singh, M.P.; Chakraborty, D.; Mukherjee, J.; Prasad, P.V.V. Balancing Water and Radiation Productivity Suggests a Clue for Improving Yields in Wheat under Combined Water Deficit and Terminal Heat Stress. *Front. Plant Sci.* **2023**, *14*, 1171479. [CrossRef] [PubMed]
54. Xiao, Z.; Zhang, N.; Zhang, Y.; Zhu, K.; Wang, W.; Zhang, W.; Gu, J.; Zhang, G.; Liu, L.; Zhang, J.; et al. Synergistic Mechanism of Moderate Wetting Drying Irrigation Improving Rice Productivity and Environmental Sustainability. *Field Crops Res.* **2025**, *332*, 110035. [CrossRef]

55. Bo, Y.; Wang, X.; Van Groenigen, K.J.; Linquist, B.A.; Müller, C.; Li, T.; Yang, J.; Jägermeyr, J.; Qin, Y.; Zhou, F. Improved Alternate Wetting and Drying Irrigation Increases Global Water Productivity. *Nat. Food* **2024**, *5*, 1005–1013. [CrossRef] [PubMed]
56. Wu, G.; Ling, J.; Liu, Z.-X.; Xu, Y.-P.; Chen, X.-M.; Wen, Y.; Zhou, S.-L. Soil Warming and Straw Return Impacts on Winter Wheat Phenology, Photosynthesis, Root Growth, and Grain Yield in the North China Plain. *Field Crops Res.* **2022**, *283*, 108545. [CrossRef]
57. Hu, M.; Zhang, D.; Du, W.; Tian, H.; Hao, Y.; Ding, S.; Yang, K.; Xu, R.; Zhang, L. Screening for Cold Tolerance Resources in Maize Seedlings and Analysis of Leaf Cell Responses. *Front. Plant Sci.* **2025**, *16*, 1565831. [CrossRef]
58. Han, Y.; Zhao, Y.; Wang, J. Unveiling Geospatial Heterogeneity in Climate's Impacts on Wheat Production to Advance Spatially-Matched Climate-Adaptive Agricultural Management in the North China Plain. *J. Environ. Manag.* **2024**, *369*, 122364. [CrossRef]